Dynamic model of cage induction motor with number of rotor bars as parameter

Gojko Joksimović

Faculty of Electrical Engineering, University of Montenegro, George Washington boulevard b.b., 81000, Podgorica, Montenegro
E-mail: Gojko.Joksimovic@ac.me

Published in *The Journal of Engineering*; Received on 1st March 2017; Accepted on 8th May 2017

Abstract: A dynamic mathematical model, using number of rotor bars as parameter, is reached for cage induction motors through the use of coupled-circuits and the concept of winding functions. The exact MMFs waveforms are accounted for by the model which is derived in natural frames of reference. By knowing the initial motor parameters for a priori adopted number of stator slots and rotor bars model allows change of rotor bars number what results in new model parameters. During this process, the rated machine power, number of stator slots and stator winding scheme remain the same. Although presented model has a potentially broad application area it is primarily suitable for the analysis of the different stator/rotor slot combination on motor behaviour during the transients or in steady-state regime. The model is significant in its potential to provide analysis of dozen of different number of rotor bars in a few tens of minutes. Numerical example on cage rotor induction motor exemplifies this application, including three variants of number of rotor bars.

Nomenclature

A_b	cross-sectional rotor bar area, m^2
A_{ers}	cross-sectional end-ring segment area, m^2
a	axial end-ring segment dimension, m
B_g	air gap flux density, T
B_{tr}	magnetic flux density in the rotor tooth, T
b	radial end-ring segment dimension, m
b_{or}	rotor slot mouth wide, m
b_{tr}	rotor teeth width, m
D_r	rotor diameter, m
d_1	rotor slot diameter 1, m
d_2	rotor slot diameter 2, m
f_1	mains supply frequency, Hz
g	air gap length, m
h_{cr}	rotor core height, m
h_{or}	rotor slot mouth height, m
h_r	rotor slot height, m
I_b	rotor bar current, rms, A
I_{ers}	end-ring segment current, *rms,* A
$\boldsymbol{i}_r$	vector of rotor loop currents, $Q_r \times 1$, A
$\boldsymbol{i}_s$	vector of stator phase currents, $m_1 \times 1$, A
J	rotor inertia, kgm^2
K_{Fe}	iron-core stacking factor, $K_{Fe} = 0.96$
k_{skew}	skew factor
k_{w1}	stator phase winding factor
L_b	rotor bar leakage inductance, H
L_{ers}	rotor end-ring segment leakage inductance, H
$\boldsymbol{L}_{rr}$	rotor inductance matrix, $Q_r \times Q_r$, H
L_{r_phase}	equivalent 'rotor phase' inductance, H
L_r'	equivalent 'rotor phase' inductance referred to stator, H
$\boldsymbol{L}_{rs}$	rotor-stator mutual inductance matrix, $Q_r \times m_1$, H
$L_{sr} = L_{rs}^T$	stator-rotor mutual inductance matrix, $m_1 \times Q_r$, H
$\boldsymbol{L}_{ss}$	stator inductance matrix, $m_1 \times m_1$, H
l	axial length of the machine, m
l_b	rotor bar length, m
l_{ers}	end-ring segment length, m
m_1	number of stator phases
$N(\theta)$	winding function, turns
$n(\theta)$	turns function, turns
p	pole pair number
Q_r	number of rotor bars
Q_s	number of stator slots
R_b	rotor bar resistance, Ω
R_{ers}	rotor end-ring segment resistance, Ω
R_{r_phase}	equivalent 'rotor phase' resistance, Ω
R_r'	equivalent 'rotor phase' resistance referred to stator, Ω
r	mean air gap radius, m
$\boldsymbol{r}_r$	matrix of rotor resistances, $Q_r \times Q_r$, Ω
$\boldsymbol{r}_s$	matrix of stator phase resistances, $m_1 \times m_1$, Ω
T_{em}	electromagnetic torque, Nm
T_L	load torque, Nm
t	time, s
$\boldsymbol{u}_s$	stator voltages vector, $m_1 \times 1$, V
w_1	stator phase series turns number
z	number of stator slots per pole per phase
γ	rotor bar skew angle, rad
θ	rotor relative angular position with respect to stator, rad
λ_b	specific rotor bar permeance
λ_{ers}	specific end-ring segment permeance
μ_0	free space permeability, $\mu_0 = 4\pi \cdot 10^{-7}$, H/m
τ_r	rotor slot pitch, m
$\boldsymbol{\psi}_s$	stator flux linkage vector, $m_1 \times 1$, Wb
$\boldsymbol{\psi}_r$	rotor flux linkage vector, $Q_r \times 1$, Wb
ω_1	mains supply angular frequency, rad/s
ω_r	rotor speed, rad/s

1 Introduction

Perhaps the earliest established model for induction motors in a natural frame of reference and using a multiple coupled circuit approach was published in the famous work by Fudeh and Ong [1]. This model analysed space harmonics and their influence on motor transients. In this model, symmetrical machine was assumed. All magnetomotive forces (MMFs) in the machine are represented on the harmonic by harmonic basis – as a sum of fundamental and higher space harmonic components.

The paper by Luo *et al.* [2] moved the development of this field further, and represented a major step forward. In it, the authors presented an induction motor using winding functions, and modelled this on the basis of a multiple coupled circuit. What is now clear is that their model represents the standard for induction motors modelling, and has done so for the last two decades, notably in

relation to, a range of fault conditions and their investigation. The key feature of the model is that it can account for different winding distributions, without the nature of that winding (wound or cage winding) affecting the model. Similarly, the model makes no assumptions about symmetry or the lack of it. The space harmonics of the MMFs in the machine are considered at the same time, rather than on a harmonic by harmonic basis. It means that the exact shape of each MMF is considered, while the model also lends itself to numerical modelling. It should be noted that the model is linear in sense that it only considers the electromagnetic processes in the air-gap rather than other processes. However, the majority of models of induction machines suffer in this regard, as it is the case with conventional d–q model. The magnetic circuit and particularly its saturation can be dealt with through this model thanks to air-gap permeance modulation [3, 4], and as such the model has been employed extensively to model a range of fault conditions in both induction and synchronous machines in recent decades [5–11]. The model also provides insight into the functioning of various important higher harmonics in stator current spectrum which originate from machine design, saturation of the magnetic current and/or existence of the fault and its level [12–15]. It remains true, nonetheless, that, despite the intense use of this model for a range of investigations, there remain areas which have not yet been considered to their full extent.

It is of interest to examine the possibility of expansion and adjustment of this model for the derivation of more general cage induction motor model that will be capable to use a number of rotor bars as a parameter, and such an investigation is presented here. Some preliminary results have already been given in a recently presented paper by the same author [16].

Since the beginning of the induction motor invention and extensively utilisation, it has been clear that the number of stator slots and rotor bars, and the relationship between the two, produces a considerable effect on a variety of the cage induction motor characteristics.

The first stage in designing an induction motor is to identify its principal geometric dimensions: these include the diameter of the stator bore and the rotor, the length of the air-gap and the machine's total axial length. There follows a decision on the number of stator slots, Q_s and rotor bars, Q_r. The selection of these numbers, and their relationship, is one of the key elements of the induction motors design process. When the slot combination is inappropriate, considerable vibrations and acoustic noise can result, while in some cases, the motor may not operate at all [17]. The relationship between slots influence elements such as shape of torque-speed characteristics, leading to possible problems in operation, while at the same time altering the cost of manufacture, temperature rise and so on [18]. Having said that, it is surprising that over a century after the induction motor was first invented there is still no clarity as to the optimal rotor bars number in terms of rated operating conditions or starting torque in cases where the machine has a predetermined set-up of stator slots and pole pair number. Of course, a variety of empirical norms have been identified which provide some guidance on the issue of slot combination, although there is little consensus [19], and indeed has not been since Kron proposed the first rules in 1931 [20]. Standard textbooks and a range of published works have identified some further rules [21–24], but this authors believes that, to judge from initial analysis, the rules used are not universally applicable.

This paper aims to shed light on this issue by examining how using the number of rotor bars as the principal parameter affects the numerical model of a cage induction motor. Following the first phase of machine design, given a specified number of stator slots and rotor bars, any number of rotor bars that have sense could be used, always assuming invariant rated machine power, number of stator slots and stator winding design.

2 Induction motor model and parameters

2.1 Induction motor model

The standard mathematical model of an induction motor is widely familiar. It follows here using voltage equations, in matrix notation,

$$\boldsymbol{u}_s = \boldsymbol{r}_s \boldsymbol{i}_s + \frac{\mathrm{d}\boldsymbol{\psi}_s}{\mathrm{d}t} \tag{1}$$

$$0 = \boldsymbol{r}_r \boldsymbol{i}_r + \frac{\mathrm{d}\boldsymbol{\psi}_r}{\mathrm{d}t} \tag{2}$$

where the flux linkages are:

$$\boldsymbol{\psi}_s = \boldsymbol{L}_{ss} \boldsymbol{i}_s + \boldsymbol{L}_{sr} \boldsymbol{i}_r \tag{3}$$

$$\boldsymbol{\psi}_r = \boldsymbol{L}_{rs} \boldsymbol{i}_s + \boldsymbol{L}_{rr} \boldsymbol{i}_r \tag{4}$$

The equations for the developed electromagnetic torque and rotor speed are as follows:

$$T_{em} = \boldsymbol{i}_s^{\mathrm{T}} \frac{\mathrm{d}\boldsymbol{L}_{sr}}{\mathrm{d}\theta} \boldsymbol{i}_r \tag{5}$$

$$T_{em} - T_L = J \frac{\mathrm{d}\omega_r}{\mathrm{d}t} = J \frac{\mathrm{d}^2\theta}{\mathrm{d}t^2} \tag{6}$$

Numerical methods can quickly provide the solutions to these differential equations, where there are identifiable initial values, as is demonstrated in [4].

2.2 Model parameters

The calculation of stator winding resistances, like those of self, mutual and leakage inductances is not presented here, since they can all be reached in the usual way. The rotor parameters are the key element of the calculation.

- *Rotor winding resistances*

The winding of cage rotors, where there are Q_r rotor bars and $2Q_r$ end-ring segments might be viewed as Q_r-phase winding, assuming that one phase is formed of one rotor bar and two associated end-ring segments. There is a well-known equation to find the relationship between rms currents in the rotor bar and the end-ring segment in a machine with p pair of poles:

$$I_b = 2I_{ers} \sin\left(\frac{p\pi}{Q_r}\right) \tag{7}$$

The equivalent resistance of one rotor 'phase' is obtained from the condition of Joule power invariance:

$$R_{r\_phase} = R_b + \frac{R_{ers}}{2\sin^2(p\pi/Q_r)} \tag{8}$$

This resistance referred to the stator side of an m_1-phase machine is,

$$R'_r = \frac{4m_1}{Q_r} \left(\frac{k_{w1} w_1}{k_{skew}}\right)^2 R_{r\_phase} \tag{9}$$

where $k_{w1}w_1$ represents the effective series turns number of the stator phase winding and k_{skew} is the fundamental harmonic skew factor. In the most frequent cases, being where the rotor bars are skewed for one stator slot pitch, the value of this factor is as follows:

$$k_{skew} = \frac{Q_s}{p\pi} \sin\left(\frac{p\pi}{Q_s}\right) \tag{10}$$

The resistance calculated in (9) is one which happens in a one phase steady-state equivalent circuit of an induction machine.

Having said that, this paper observes the motor in the natural frame of reference, meaning that the matrix of cage rotor resistances is a square matrix of dimension $Q_r \times Q_r$. The entries are $R_1 = 2(R_b + R_{ers})$ and $R_2 = -R_b$, where R_b and R_{ers} represent the rotor bar and end-ring segment resistances, respectively:

$$\boldsymbol{r}_r = \begin{bmatrix} R_1 & R_2 & 0 & 0 & \dots & R_2 \\ R_2 & R_1 & R_2 & 0 & \dots & 0 \\ 0 & R_2 & R_1 & R_2 & \dots & 0 \\ \dots & \dots & \dots & \dots & \dots & \dots \\ \dots & \dots & \dots & \dots & \dots & \dots \\ R_2 & 0 & 0 & 0 & \dots & R_1 \end{bmatrix}_{Q_r \times Q_r} \tag{11}$$

The known geometrical data and specific electrical conductivity of alumina mean that these resistances are easily obtained.

Given the shape of the matrix (11) and the definition of R_1 and R_2, rotor currents can clearly be identified as mesh currents, in which the mesh is formed from two neighbouring bars and associated end-ring segments. Thus the current of the rotor bar is the difference between the two neighbouring mesh currents.

- *Rotor winding inductances*

The matrix of the rotor inductances $\boldsymbol{L}_{rr}$ is also of $Q_r \times Q_r$ dimension,

$$\boldsymbol{L}_{rr} = \begin{bmatrix} L_1 & L_2 & L_3 & L_3 & \dots & L_2 \\ L_2 & L_1 & L_2 & L_3 & \dots & L_3 \\ L_3 & L_2 & L_1 & L_2 & \dots & L_3 \\ \dots & \dots & \dots & \dots & \dots & \dots \\ \dots & \dots & \dots & \dots & \dots & \dots \\ L_2 & L_3 & L_3 & L_3 & \dots & L_1 \end{bmatrix}_{Q_r \times Q_r} \tag{12}$$

where the elements are $L_1 = L_{self} + 2(L_b + L_{ers})$, $L_2 = L_{mutual} - L_b$ and $L_3 = L_{mutual}$.

The self-inductance of the rotor loop L_{self}, as well as the mutual inductance between two rotor loops L_{mutual} is easily found by considering the definition of the winding function [2]:

$$L_{self} = \frac{\mu_0 r l}{g} \frac{2\pi}{Q_r^2} (Q_r - 1) \tag{13}$$

$$L_{mutual} = -\frac{\mu_0 r l}{g} \frac{2\pi}{Q_r^2} \tag{14}$$

Thus it is a simple task to calculate, the main power of winding function approach through these inductances, without reference to the number of rotor bars.

The leakage inductance values L_b and L_{ers} are dependent on the rotor bars and the end-ring segments, and specifically their dimensions and shape. The initial machine design provides the cross-sectional area of the rotor bars, A_b. If we adopt a bar shape as shown by Fig. 1, we can ensure that there is a constant rotor teeth width b_{tr} for the entire length of the tooth.

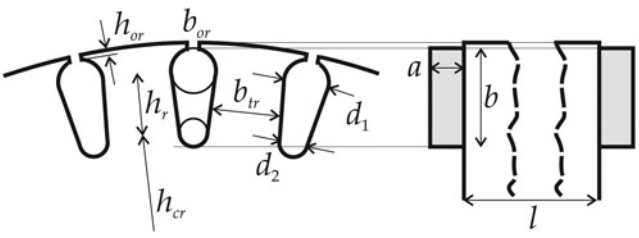

Fig. 1 *Shape and dimensions of the rotor bar and the end-ring*

It is thus easy to calculate the following dimensions of the rotor slot, for Q_r rotor bars,

$$d_1 = \frac{\pi(D_{er} - 2h_{or}) - Q_r b_{tr}}{\pi + Q_r} \tag{15}$$

$$d_2 = \sqrt{\frac{8CA_b - (C\pi + 8)d_1^2}{C\pi - 8}} \tag{16}$$

$$h_r = \frac{d_1 - d_2}{2\tan \pi/Q_r} \tag{17}$$

where:

$$b_{tr} \cong \frac{B_g}{K_{Fe} B_{tr}} \tau_r = \frac{B_g \pi D_r}{K_{Fe} B_{tr} Q_r} \tag{18}$$

$$C = 4\tan\frac{\pi}{Q_r} \tag{19}$$

The rotor end-ring dimensions are calculated on the basis of the initial machine design process, where the end-ring height b, is,

$$b = (1 \div 1.2) \cdot (h_{or} + h_r + 0.5(d_1 + d_2)) \tag{20}$$

while the other dimension is:

$$a = \frac{A_{ers}}{b} \tag{21}$$

Once we have the rotor slot and end-ring dimensions, we can then find the appropriate leakage inductances [23]:

$$L_b = \mu_0 l_b \lambda_b \cong \mu_0 l_b \left(0.66 + \frac{2h_r}{3(d_1 + d_2)} + \frac{h_{or}}{b_{or}}\right) \tag{22}$$

$$L_{ers} = \mu_0 l_{ers} \lambda_{ers} = \mu_0 \cdot \frac{\pi(D_r - b)}{Q_r} \cdot \left[0.46 \cdot \log\left(\frac{2.35 \cdot (D_r - b)}{2a + b}\right)\right] \tag{23}$$

One useful element is to find the connection between the above parameters and that found in single phase equivalent circuit as for resistances. Through magnetic energy invariance, we can identify the equivalent inductance of one cage rotor 'phase' as,

$$L_{r\_phase} = L_b + \frac{L_{ers}}{2\sin^2(p\pi/Q_r)} \tag{24}$$

while the value referred to the stator side of m_1-phase machine is:

$$L'_r = \frac{4m_1}{Q_r} \left(\frac{k_{w1} w_1}{k_{skew}}\right)^2 L_{r\_phase} \tag{25}$$

This is the inductance that takes place in a one phase steady-state equivalent circuit of the induction machine. In this case, it occurs as leakage reactance:

$$X'_r = \omega_1 L'_r = 2\pi f_1 L'_r \tag{26}$$

- *Stator-rotor mutual inductance*

Mutual inductance between the stator phase and rotor loop is one of the essential parameters in this model. This inductance is time dependent i.e. it varies with the rotor position. Given a known winding function of stator phase, say phase A, the mutual inductance is found through iterative processes of the numerical integration of the following integral,

$$L_{sAr1} = \frac{\mu_0 r l}{g} \int_0^{2\pi} N_A(\theta) \cdot n_{r1}(\theta)\, d\theta \tag{27}$$

while the turns function of rotor loop, say loop 1, finds its position altered slightly for one rotor revolution. Thus a look-up table can be found so that the appropriate mutual inductance value can be identified for any given angle of a rotor position.

Since the motor is symmetrical, all that is required is to identify the mutual inductance between one stator phase and one rotor loop. Once this is done, the mutual inductance for one rotor position is available from the look up table once appropriate shifting has been taken into account, regardless of the loop or stator phase in question.

3 Changes to the number of rotor bars

The initial design process of the machine, described in [23], involves deciding the principal machine dimensions, the number of stator slots and rotor bars, and the stator and the rotor cage winding parameters. Of course, the quantity of stator slots Q_s is essentially fixed and derives from the motor dimensions: invariably, it is the product of number of slots per pole per phase z, the number of phases m_1 and the number of poles $2p$, $Q_s = 2 \cdot z \cdot m_1 \cdot p$.

To alter the number of rotor bars, while leaving the stator unchanged, the rotor bar cross-section area is changed. This naturally assumes that the machine has a fixed rated power and that current density in rotor bars remains the same. In order that the machine develops the same power at the same slip, the following equality must hold true,

$$Q_r R_b I_b^2 = Q_{r\_new} R_{b\_new} I_{b\_new}^2 \tag{28}$$

or

$$Q_r R_b \left(\xi \frac{2k_{w1} w_1 m_1}{Q_r} I_{1rated} \right)^2 = Q_{r\_new} R_{b\_new} \left(\xi \frac{2k_{w1} w_1 m_1}{Q_{r\_new}} I_{1rated} \right)^2 \tag{29}$$

where:

$$\xi \cong 0.8 \cdot \cos \varphi_{rated} + 0.2 \tag{30}$$

Thus it follows,

$$R_{b\_new} = \frac{Q_{r\_new}}{Q_r} R_b \tag{31}$$

$$A_{b\_new} = \frac{Q_r}{Q_{r\_new}} A_b \tag{32}$$

$$R_{ers\_new} = \frac{R_{ers}}{\alpha} \tag{33}$$

where,

$$\alpha = \frac{Q_{r\_new} A_{ers\_new}}{Q_r A_{ers}} \tag{34}$$

Once we know what the cross section area values are as a result of this, we can identify both the rotor slot and the end-ring dimensions, meaning that new leakage inductance values can be calculated through (22) and (23).

4 Results and discussion

Tables 1 and 2 provide results for machine parameters for a three-phase induction machine with the following rated values: $P_n = 11$ kW, $U_n = 400$ V, $f = 50$ Hz, $n_n = 735$ rpm, wye connection, which has a targeted rated power factor and rated efficiency of $\cos\varphi_n = 0.7$, $\eta_n = 0.9$, when there are $Q_s = 48$ stator slots and $Q_r = 30$ rotor bars.

As in the procedure explained above, when we use two new numbers of rotor bars, $Q_r = 33$ and $Q_r = 40$, distinct new dynamic model parameters are found. They are provided in Tables 3 and 4:

The stator winding remains unchanged in all cases, as does the fact that the rotor bars are skewed at an angle of one stator tooth pitch, $\gamma = 2\pi/Q_s$ [25]. The figure below provides the results for three separate rotor bar numbers after numerical modelling.

Fig. 2 shows the waveforms of mutual inductance between stator phase and rotor loop for three separate rotor bar numbers. The results, as expected, show that greater rotor bar numbers, meaning a smaller loop width, produce smaller mutual inductance amplitudes.

Fig. 3 shows the motor's electromagnetic torque, created during unloaded start-up. It is clear that a machine with $Q_r = 40$ bars produces the most significant torque peaks, which means that this set-up allows the machine to achieve a steady state regime most quickly. It is also clear that all the machines are loaded with rated load at $t = 0.6$ s.

Table 1 Steady state equivalent circuit parameters for initial design, $Q_s = 48$, $Q_r = 30$

$P_n = 11$ kW, $U_n = 400$ V, $f = 50$ Hz, $n_n = 735$ rpm, wye, $\cos\varphi_n = 0.7$, $\eta_n = 0.9$, $Q_s = 48$, $Q_r = 30$	
stator phase winding resistance, R_s	0.222 Ω
stator phase winding leakage reactance, X_{sl}	0.679 Ω
magnetising reactance, X_m	12.77 Ω
rotor phase winding resistance, referred to stator, R'_r	0.293 Ω
rotor phase winding leakage reactance, referred to stator, X'_r	0.485 Ω

Table 2 Dynamic model parameters for initial design, $Q_s = 48$, $Q_r = 30$

$P_n = 11$ kW, $U_n = 400$ V, $f = 50$ Hz, $n_n = 735$ rpm, wye, $\cos\varphi_n = 0.7$, $\eta_n = 0.9$, $Q_s = 48$, $Q_r = 30$	
stator phase winding resistance, R_s	0.222 Ω
stator phase winding leakage inductance, L_{sl}	2.162 mH
rotor bar resistance @80°C, R_b	77.394 μΩ
rotor end-ring segment resistance @80°C, R_{rs}	4.569 μΩ
rotor bar leakage reactance, L_b	445.067 nH
rotor end-ring segment leakage reactance, L_{rs}	11.988 nH

Table 3 Dynamic model parameters for new design, $Q_s = 48$, $\boldsymbol{Q_r = 33}$

$P_n = 11$ kW, $U_n = 400$ V, $f = 50$ Hz, $n_n = 735$ rpm, wye, $\cos\varphi_n = 0.7$, $\eta_n = 0.9$, $Q_s = 48$, $\boldsymbol{Q_r = 33}$	
stator phase winding resistance, R_s	0.222 Ω
stator phase winding leakage inductance, L_{sl}	2.162 mH
rotor bar resistance @80°C, R_b	85.133 μΩ
rotor end-ring segment resistance @80°C, R_{rs}	4.175 μΩ
rotor bar leakage reactance, L_b	465.43 nH
rotor end-ring segment leakage reactance, L_{rs}	11.09 nH

Table 4 Dynamic model parameters for new design, $Q_s = 48$, $\boldsymbol{Q_r = 40}$

$P_n = 11$ kW, $U_n = 400$ V, $f = 50$ Hz, $n_n = 735$ rpm, wye, $\cos\varphi_n = 0.7$, $\eta_n = 0.9$, $Q_s = 48$, $\boldsymbol{Q_r = 40}$	
stator phase winding resistance, R_s	0.222 Ω
stator phase winding leakage inductance, L_{sl}	2.162 mH
rotor bar resistance @80°C, R_b	103.19 μΩ
rotor end-ring segment resistance @80°C, R_{rs}	3.471 μΩ
rotor bar leakage reactance, L_b	511.82 nH
rotor end-ring segment leakage reactance, L_{rs}	9.185 nH

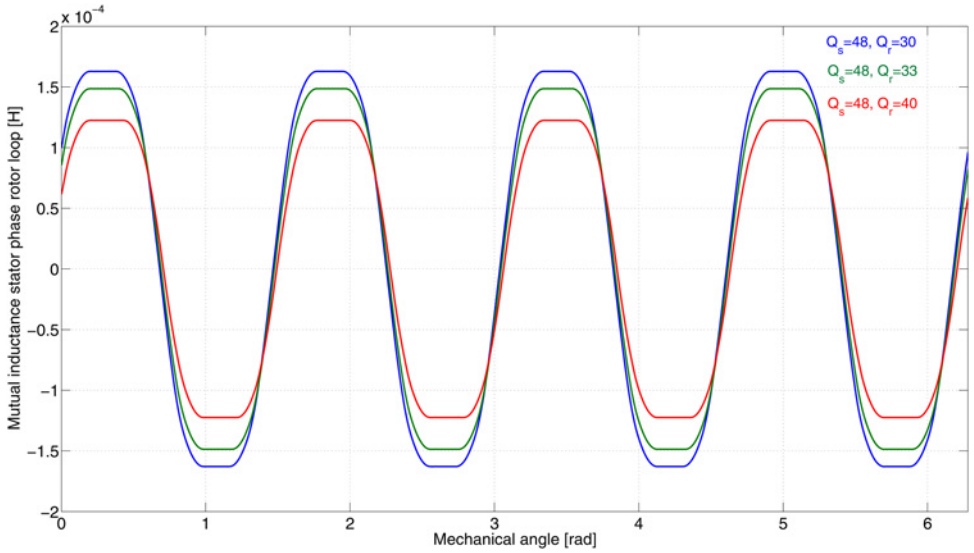

Fig. 2 *Stator phase – rotor loop mutual inductance waveform for three different number of rotor bars: $Q_s = 48$, $Q_r = 30$, 33 and 40. Rotor bars are skewed for $\gamma = 2\pi/Q_s$, [rad]*

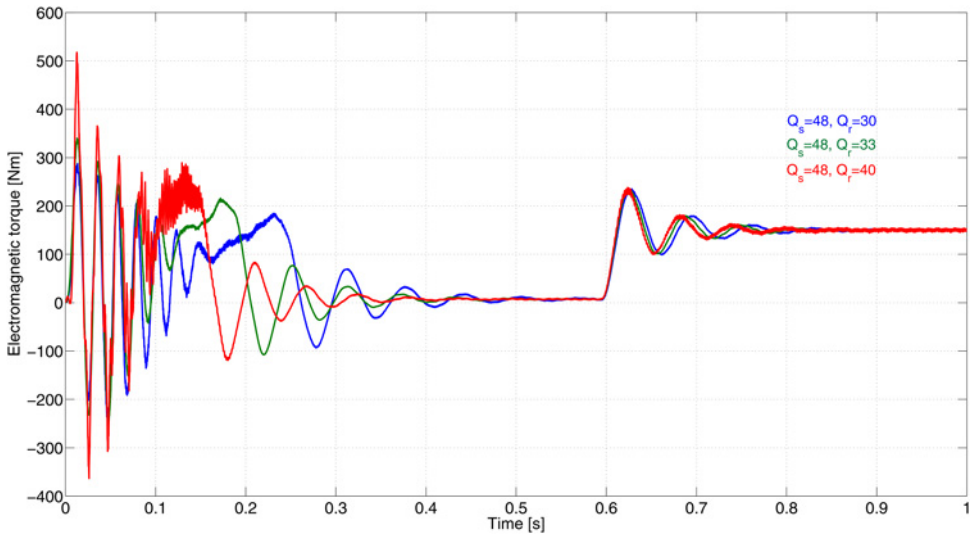

Fig. 3 *Developed electromagnetic torque of the machine during no-load start-up. The machine is loaded with a rated load at $t = 0.6$ s*

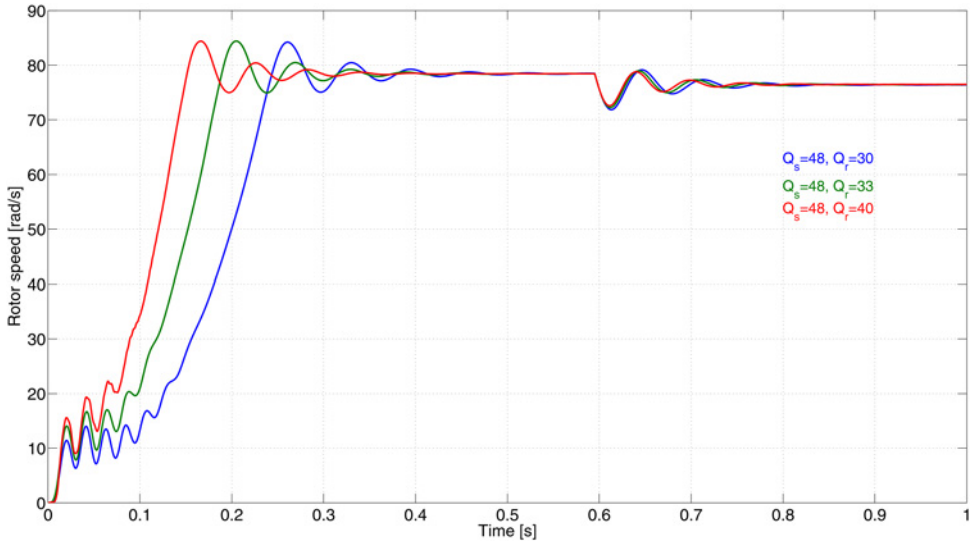

Fig. 4 *Rotor speed during no-load start-up. The machine is loaded with a rated load at $t = 0.6$ s*

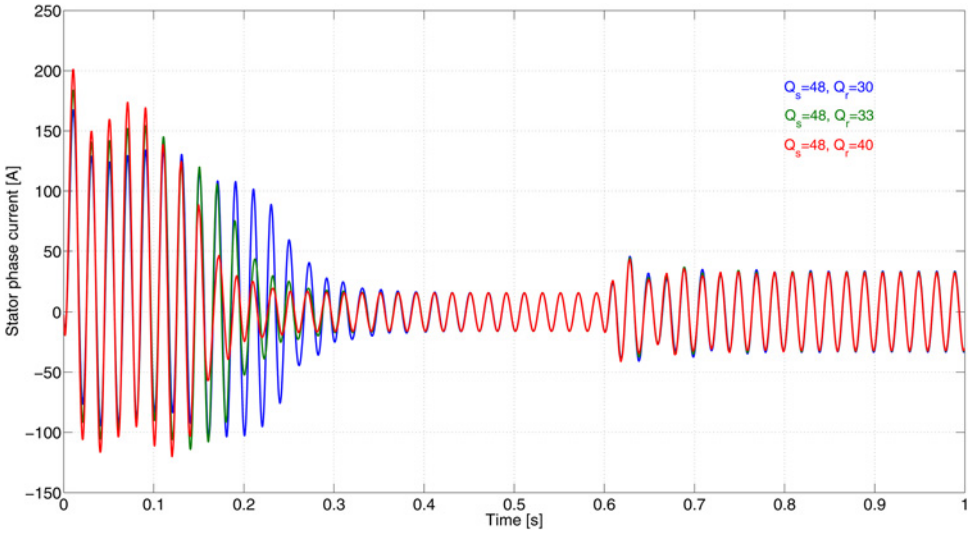

Fig. 5 *Stator phase current during no-load start-up. The machine is loaded with a rated load at t = 0.6 s*

Fig. 4 provides machine rotor speed in the same conditions. It is evident that rotor speed is closely related to developed electromagnetic torques, i.e. the machine with $Q_r = 40$ bars run-up fastest, with the rotor speeds being exactly the same in a steady state regime. The same holds for the stator phase current values shown in Fig. 5.

Fig. 6 shows the current waveforms in one rotor bar as part of the same transient process. This current represents the difference between the currents in the two neighbouring rotor loops that make up two rotor bars and their corresponding end-ring segments.

On the basis of these figures, it is clear that the optimal rotor choice of the three would be a rotor with $Q_r = 40$ bars, which has the greatest starting torque. The results given in Fig. 7, by contrast, demonstrate that the same rotor ($Q_r = 40$ rotor bars) provides the worst performance in a steady state regime, because of the extreme pulsations of electromagnetic torque it produces. As such, a machine with $Q_r = 33$ rotor bars offers the best steady state regime performance, even if there is a low-frequency torque harmonic component in this case.

The example given above, featuring three different number of rotor bar choices, demonstrates just how complicated the choice of rotor bar number, and indeed their combination with stator slots, actually is. Where one option provides better starting torque, it might perform badly in steady state regime. The choice is clear; it is possible to have good starting torque or good steady state performance, but in the most practical cases not both. This model helps in the decision process between these two options, quickly and reliably.

5 Conclusion

This paper offers a tool of significant interest and utility for cage induction motor designers and the wider scientific community in relation to the design and application of induction machines. The model produces a time series of rotor speed, electromagnetic torque, stator and rotor currents, all of which can be considered for any sensible number of rotor bars. The numerical example highlights the power of the model. By analysing three randomly selected numbers of rotor bars, we have demonstrated that various solutions are not acceptable, because of the extent of the electromagnetic pulsations in the steady state regime.

The model allows for the consideration of any number of pole pairs, stator slots and rotor bars in any combination, as well as for any type of stator winding design. The model's key benefit is in allowing the analysis of numerous combinations extremely quickly: ten or more different number of rotor bars requires only

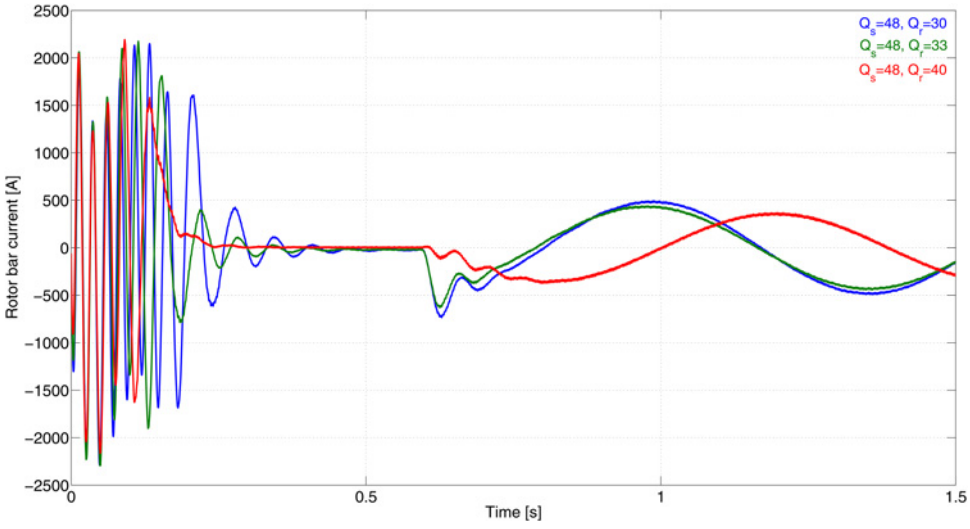

Fig. 6 *Rotor bar current during no-load start-up. The machine is loaded with a rated load at t = 0.6 s*

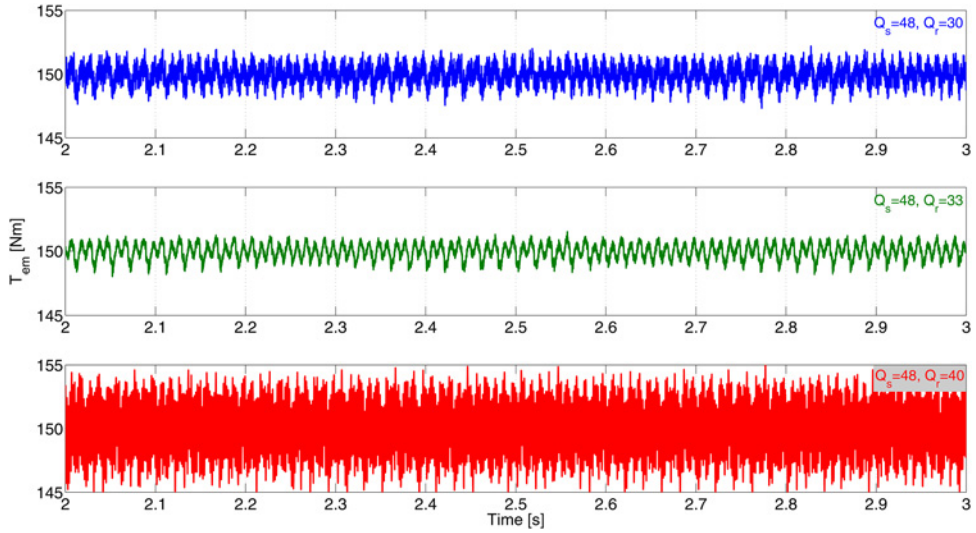

Fig. 7 *Developed electromagnetic torque in a steady state. The machine is loaded with a rated load*

few tens of minutes for full analysis, which is a significant advantage in comparison to finite element method models. Assuming the right criteria are employed, something which remains under investigation, we should soon be able to identify the precise, optimal number of rotor bars required for a given number of stator slots and pole pairs.

This analysis has considered a line-fed, symmetrical wye connected three phase cage induction motor. The same process might be applied either to single phase or multiphase machines. Additionally, there are no any restrictions in the sense that model can be used for delta connected or inverter-fed machines.

6 References

[1] Fudeh H.R., Ong C.M.: 'Modeling and analysis of induction machines containing space harmonics', *IEEE Trans. PAS*, 1983, **102**, (8), pp. 2608–2615

[2] Luo X., Liao Y., Toliyat H.A., *ET AL.*: 'Multiple coupled circuit modeling of induction machines', *IEEE Trans. Ind. Appl.*, 1995, **31**, (2), pp. 311–318

[3] Nandi S.: 'A detailed model of induction machines with saturation extendable for fault analysis', *IEEE Trans. Ind. Appl.*, 2004, **40**, (5), pp. 1302–1309

[4] Joksimović G.: 'Line current spectrum analysis in saturated three-phase cage induction machine', *Electr. Eng.*, 2010, **91**, (8), pp. 425–437

[5] Nandi S., Toliyat H.A., Li X.: 'Condition monitoring and fault diagnosis of electrical motors – a review', *IEEE Trans. Energy Convers.*, 2005, **20**, (4), pp. 719–729

[6] Tabatabaei I., Faiz J., Lesani H., *ET AL.*: 'Modeling and simulation of a salient-pole synchronous generator with dynamic eccentricity using modified winding function theory', *IEEE Trans. Magn.*, 2004, **40**, (3), pp. 1550–1555

[7] Joksimović G., Penman J.: 'The detection of inter-turn short circuits in the stator windings of operating motors', *IEEE Trans. Ind. Electron.*, 2000, **47**, (5), pp. 1078–1084

[8] Bruzzese C., Joksimović G.: 'Harmonic signatures of static eccentricities in the stator voltages and in the rotor current of no-load salient-pole synchronous generators', *IEEE Trans. Ind. Electron.*, 2011, **58**, (5), pp. 1606–1624

[9] Faiz J., Ojaghi M.: 'Unified winding function approach for dynamic simulation of different kinds of eccentricity faults in cage induction machines', *IET Electr. Power Appl.*, 2009, **3**, (5), pp. 461–470

[10] Joksimović G., Đurović M., Penman J., *ET AL.*: 'Dynamic simulation of dynamic eccentricity in induction machines–winding function approach', *IEEE Trans. Energy Convers.*, 2000, **15**, (2), pp. 143–148

[11] Joksimović G.: 'Dynamic simulation of cage induction machine with air gap eccentricity', *IEE Proc., Electr. Power Appl.*, 2005, **152**, (4), pp. 803–811

[12] Nandi S., Ahmed S., Toliyat H.A.: 'Detection of rotor slot and other eccentricity related harmonics in a three phase induction motor with different rotor cages', *IEEE Trans. Energy Convers.*, 2001, **16**, (3), pp. 253–260

[13] Joksimović G.M., Riger J., Wolbank T.M., *ET AL.*: 'Stator-current spectrum signature of healthy cage rotor induction machines', *IEEE Trans. Ind. Electron.*, 2013, **60**, (9), pp. 4025–4033

[14] Joksimović G.: 'AC winding analysis using winding function approach', *Int. J. Electr. Eng. Educ.*, 2011, **48**, (1), pp. 34–52, (19)

[15] Joksimović G., Đurović M., Penman J.: 'Cage rotor MMF–winding function approach', *IEEE Power Eng. Rev.*, 2001, **21**, (4), pp. 64–66

[16] Joksimović G.: 'Parameterized dynamic model of cage induction machine'. XXII Int. Conf. on Electrical Machines, ICEM 2016, Lausanne, Switzerland, September 2016

[17] Kobayashi T., Tajima F., Ito M., *ET AL.*: 'Effects of slot combination on acoustic noise from induction motors', *IEEE Trans. Magn.*, 1997, **33**, (2), pp. 2101–2104

[18] Nailen R.L.: 'The importance of 'slot combination' in a-c motor design', *Electr. Appar.*, 2005, **45**, (8), pp. 3131–3136

[19] Besnerais J.L., Lanfranchi V., Hecquet M., *ET AL.*: 'Optimal slot numbers for magnetic noise reduction in variable-speed induction motors', *IEEE Trans. Magn.*, 2009, **45**, (8), pp. 3131–3136

[20] Kron G.: 'Induction motor slot combinations: rules to predetermine crawling vibrations, noise and hooks in the speed-torque curve', *AIEE Trans.*, 1931, **50**, (2), pp. 757–767

[21] Oberretl K.: 'The effect of parallel winding, delta connection, pitch, sloth width and slot skew on the torque of squirrel-cage motors', *Elektrotech. Z. A*, 1965, **86**, pp. 609–614

[22] Alger P.: 'Induction machines: their behavior and uses' (Gordon and Breach Science Publishers, 1970)

[23] Boldea I., Nasar S.A.: 'The induction machine handbook' (CRC Press, 2002)

[24] Richter R.: 'Elektrische Maschinen' (Die Induktionsmaschine, Verlag Birkhauser, 1954), vol. **4**

[25] Joksimović G.M., Đurović M.D., Obradović A.B.: 'Skew and linear rise of MMF across slot modeling – winding function approach', *IEEE Trans. Energy Convers.*, 1999, **14**, (3), pp. 315–320

7 Appendix

Stator phase winding scheme:

A-1-6′-2-7′-13-8′-12-7′-13-18′-14-19′-25-20′-24-19′-25-30′-26-31′-37-32′-36-31′-37-42′-38-43′-1-44′-48-43′-X